Controlling the mode profile of photonic crystal nanobeam cavities with mix-and-match unit cells

SAMI I. HALIMI,[1,†] ZHONGYUAN FU,[2,†] FRANCIS O. AFZAL,[1] JOSHUA A. ALLEN,[3] SHUREN HU,[1,4] AND SHARON M. WEISS[1,3,4,*]

[1]Department of Electrical Engineering and Computer Science, Vanderbilt University, Nashville, Tennessee 37235, USA
[2]State Key Laboratory of Information Photonics and Optical Communications, School of Information and Communication Engineering, Beijing University of Posts and Telecommunications, Beijing 100876, China
[3]Interdisciplinary Graduate Program in Materials Science, Vanderbilt University, Nashville, Tennessee 37235, USA
[4]Department of Physics and Astronomy, Vanderbilt University, Nashville, Tennessee 37235, USA
*Corresponding author: sharon.weiss@vanderbilt.edu

[†]These authors contributed equally

Received XX Month XXXX; revised XX Month, XXXX; accepted XX Month XXXX; posted XX Month XXXX (Doc. ID XXXXX); published XX Month XXXX

We report simulations and experimental measurement of a photonic crystal (PhC) designed with different unit cell geometries in a single device. This "mix-and-match" approach enables enhanced mode manipulation by incorporating non-traditional unit cell shapes into a one-dimensional PhC nanobeam cavity. Inclusion of a bowtie-shaped unit cell in the center of a mix-and-match PhC nanobeam cavity comprised elsewhere of either circular or antislot unit cells leads to a two order of magnitude reduction in the mode volume of the cavity while maintaining a similar quality factor.

http://dx.doi.org/10.1364/AO.99.099999

1. INTRODUCTION

For many applications in photonics, having a high degree of light-matter interaction is essential. In some of these applications, having a low-loss resonance is important, the metric for which is the quality factor (Q), while other applications rely on having high peak energy density and low modal volume (V_m). Photonic crystal (PhC) cavities have been demonstrated in a wide range of on-chip applications for light-matter interaction, including optical modulators [1,2], lasers [3,4], and optical biosensors [5,6]. While the Q of PhCs can be tuned over a large range ($Q \sim 10^2 - 10^6$) in a straightforward manner by changing the number of unit cells and the dimensions thereof, it remains difficult to manipulate the mode distribution and energy density across the unit cells. Ultimate control of the performance of resonant PhC devices requires tuning both Q and V_m independently, as some applications are impaired by too high a Q (e.g., ultrafast switching). In these cases, ultralow V_m and modest Q may be ideal. Recent work has demonstrated it is possible to leverage subwavelength design for subwavelength mode concentration in PhC cavities [7–9]. The antislot and bowtie unit cells redistribute light within the unit cell to critical dimensions near 50 nm and 10 nm, respectively [7,9]. However, these designs localize the field to very small regions across all unit cells. For applications leveraging optical nonlinearities or single photon emitters, for example, it may not be desirable for multiple unit cells near the central cavity unit cell to support extremely high light intensity. Consequently, another design approach that allows control over the mode distribution across all unit cells of PhC is needed. Furthermore, PhC cavities with subwavelength features in all unit cells (e.g., Fig. 1(a)) are difficult to fabricate at scale with high fidelity, as minor fluctuations in process conditions can greatly impact the uniformity of features near the lithographic limit, with this effect being more pronounced the more of these small features are present. It is, thus, advantageous to use the minimum number of subwavelength features necessary to achieve the desired mode confinement alongside more fabrication-tolerant traditional PhC unit cells. For example, at the foundry level, fabrication of one bowtie unit cell would allow more control over the uniformity and could be more easily realized than a series of twenty or more bowtie unit cells in a single PhC device. This general approach of considering inclusion of PhC unit cells of different shapes has been followed in 1D PhCs with an air slot in the center of the cavity [10] and has been recently proposed [11,12] and experimentally reported [11] with a 1D PhC possessing a single bowtie unit cell in the center of the cavity. However, fundamental design rules to realize optimal performance metrics in such mixed unit cell PhCs have not been established. Here, we report a design methodology that can mix and match fabrication-tolerant unit cells with a subwavelength-critical unit cell, harnessing the positive attributes of subwavelength mode concentration while greatly improving the ease of fabrication and achieving much broader control of the mode distribution across all PhC unit cells.

In the conventional PhC design approach, all unit cells in a PhC have the same shape (e.g., circles, rectangles); cavities are formed by tapering

the PhC unit cells between highly mirroring regions and the cavity region to ensure a smooth transition and minimize abrupt changes between unit cells (e.g., by gradually changing the unit cell radius, lattice spacing, or nanobeam width), enabling a Gaussian field profile with low scattering losses [13,14]. Figure 1(a) shows an illustration of a bowtie PhC cavity designed in this traditional way with one unit cell geometry (i.e., the bowtie) being tapered in size across the nanobeam. In the mix-and-match unit cell design approach introduced in this work, we demonstrate that it is possible to add a single unit cell with a subwavelength-sized critical feature to an otherwise traditionally designed PhC nanobeam without incurring significant scattering losses if appropriate care is taken in selecting the unit cell radius and width. While this work introduces an approach for designing mixed unit cell PhCs by using two distinct unit cell geometries, we believe it is possible to incorporate additional unit cell geometries at different locations in the PhC through a similar design procedure, allowing fine manipulation of the mode distribution and some control over the local phase and amplitude of light within the PhC. Therefore, the design freedom afforded by mixing and matching unit cells could facilitate, for example, spatially multiplexed biosensing, directional light emission, and other new avenues for PhC functionality.

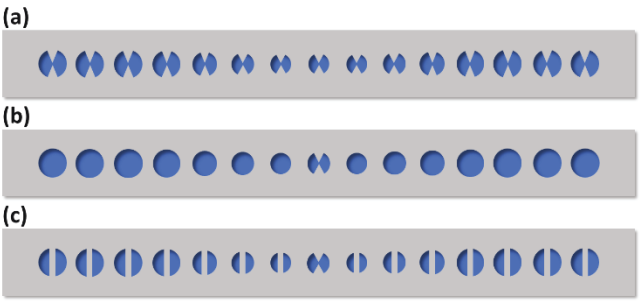

Fig. 1. Schematic illustration of (a) 1D PhC composed of bowtie unit cells, (b) mix-and-match PhC with a single bowtie unit cell at the center of the cavity, surrounded by circular air hole unit cells forming the mirrors, and (c) mix-and-match PhC with bowtie cavity unit cell and antislot mirror unit cells.

2. DESIGN APPROACH AND NUMERICAL RESULTS

The design process for the "mix-and-match" method consists of two primary steps: a "mix" step and a "match" step. In the mix step, the shape of the default unit cells is first determined. Default unit cells are typically chosen to have large, easy-to-fabricate features such as circles or rectangles. Second, the geometries of the functional unit cells are identified. Functional unit cells are chosen to have unique shapes for specialized purposes, such as subwavelength mode concentration, opto-mechanics, or polarization control. The "match" step follows an empirical optimization approach to simultaneously reduce mismatch between the band structures of both types of unit cells in k-space and between their spatial mode profiles [15,16]. This matching process can be accomplished in simulation through multi-dimensional parameter sweeps, which typically require at least two tuning parameters to be able to effectively meet the matching condition and reduce scattering losses. Here, we first adopt a brute-force simulation approach to allow full insight on the effect of different physical parameters on the optical properties of the mixed unit cell PhC to be revealed. In general, other optimization strategies may be desirable depending on the nature of the functional unit cell parameters being tuned and how much is known *a priori* about the topology of the parameter space being explored (e.g. approximate maximum location from theory or the existence of local maxima). Accordingly, after gaining knowledge of the topology of the parameter space explored for the mixed unit cell PhCs, we subsequently demonstrate that a gradient optimization approach can be used to find near-optimal design solutions in a computationally efficient manner.

To facilitate maximum control over functional unit cells with subwavelength features, an air-mode PhC, whose resonance of interest is near the air band edge, is utilized for demonstrating the mix-and-match approach. Air-mode PhCs localize light within the low-index air hole region of the unit cells [17], and electromagnetic boundary conditions can then be exploited to dictate how modal energy is distributed within the unit cell [7]. In this way, subwavelength features can be introduced in the air holes to provide a greater degree of control over the modal distribution in those unit cells. For example, a subwavelength feature such as a bowtie can further localize and confine light within a PhC, establishing two levels of optical confinement in which the air-mode design concentrates modal energy in the air holes of the lattice and then the dielectric bowtie inside the air hole effectively "funnels" the light to the tips of the bowtie. Similarly, an antislot unit cell can localize modal energy inside a high-index, vertical dielectric bar spanning an air hole, based on an interface effect that functions as the opposite of the slot effect [7,18]. Operationally, when utilizing the fundamental resonance of an air-mode PhC cavity, the central cavity unit cell is the most impactful unit cell to substitute with a functional unit cell. It is also the most straightforward to change to a functional unit cell using the mix-and-match approach.

To demonstrate the mix-and-match design technique, we designed two mixed unit cell PhC nanobeams having a bowtie-shaped functional unit cell as the central cavity unit cell, one with circular air holes as the default PhC unit cells and the other with antislots as the default unit cells, as shown in Figure 1(b-c). We note that other unit cell shapes could have been utilized without a loss of generality in the mix-and-match design approach. Three-dimensional finite-difference time-domain (FDTD) simulations (Lumerical Inc.) were first carried out to design circular air hole and antislot PhC nanobeams composed of unit cells of uniform shape, following established deterministic design procedures [14]. Band edge calculations were done to determine the desired radii of the central cavity unit cell and maximum mirror strength segments for each PhC nanobeam. The number of mirror segments between the central cavity unit cell and unit cells with maximum mirror strength (i.e., the taper length) was chosen to produce a fundamental resonance with $Q \geq 10^4$ at an appropriate near-infrared, telecom-band wavelength with sufficiently high transmission through the nanobeam to be easily measurable in experiment [19]. The resulting simulated circular air hole PhC cavity had a nanobeam width of 700 nm and period of 400 nm with 9 tapering mirror segment pairs ranging from 93 – 135 nm in radius and 5 maximum mirror strength unit cells at each end. The fundamental air-mode resonance of the circular air hole PhC cavity has a simulated $Q = 7.9\times10^4$ and $V_m = 1.5\times10^{-2}\ (\lambda/n_{air})^3$ at 1520 nm. The antislot PhC cavity was designed with a nanobeam width of 700 nm, period of 450 nm, 15 mirror pairs with radius 160 – 181 nm, and 5 maximum mirror strength unit cells. The dielectric bridges of the antislot segments were designed to be 50 nm wide. We note that introducing an antislot into the air hole of the unit cell lowers the index contrast between that air hole and the adjacent dielectric region, consequently shrinking the size of the band gap; accordingly, we increased the period of the antislot PhC to counteract this effect. The fundamental resonance of the antislot PhC cavity has a simulated $Q = 9.4\times10^4$ and $V_m = 2.8\times10^{-2}\ (\lambda/n_{air})^3$ at 1549 nm. Following this initial optimization, a single bowtie unit cell was inserted into each of the uniform PhC cavity designs, replacing the default unit cell at the center of the cavity with the goal of reducing the cavity mode volume while maintaining a similar Q. The bowtie radius and bowtie unit cell width were varied in a parameter sweep in 3D-FDTD simulations while keeping all other dimensions the same to

evaluate the resulting effect on the mixed unit cell Q and V_m. We note that changing these parameters of the bowtie unit cell do not strongly influence mode volume since the energy redistribution due to the bowtie is not a resonant effect; while the bowtie angle and gap size may affect V_m, we do not sweep those parameters here. We further note that while the radius and width of the functional unit cell are the parameters varied in the "match" step in this work, the desired application of the mixed unit cell PhC should dictate the selected shape of the functional unit cell, and dimensions of the PhC that are most impactful to the desired application should be varied.

For both mixed unit cell PhC designs, a coarse sweep over a wide range of parameters (4 nm step size in radius and unit cell width values) was performed to find the region in parameter space with maximum Q before refining the sweep to a 1 nm step size to settle on a single optimized bowtie radius and unit cell width for each design. Figure 2 shows the results of the larger step size parameter sweeps, both in calculated Q and resonant wavelength.

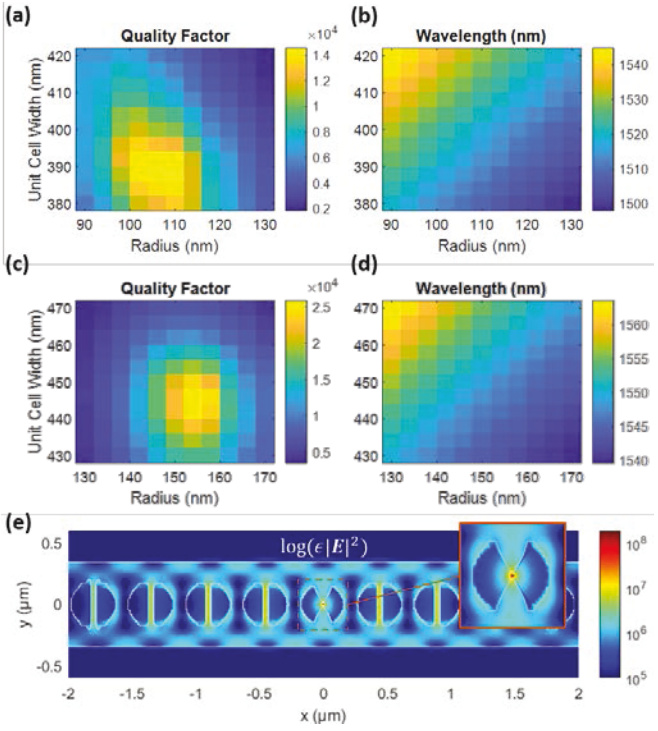

Fig. 2. Simulated 3D-FDTD parameter sweep of bowtie radius and unit cell width in (a-b) air hole-bowtie and (c-d) antislot-bowtie PhC nanobeams, showing how quality factor and resonant wavelength vary for each combination of parameters. (e) Simulated mode profile of the optimized antislot-bowtie mix-and-match PhC design.

This sweep reveals a continuous and smooth dependence of Q on radius and unit cell width along with a single local maximum. This knowledge of the design space topology can be exploited to improve computational efficiency by leveraging appropriate optimization methods that explore a subset of the parameter space while respecting its shape and continuity. Numerical optimization methods such as particle swarm optimization (PSO) and gradient optimization (GO) have been popular in recent literature for optimizing photonic devices [20–24]. While PSO is effective at avoiding local minima that may exist in a parameter space, it requires many parallel simulations that coarsely span the sample space, generally requiring more computational resources than GO. While GO is less resource-intensive than PSO, it can struggle with parameter spaces that have multiple local extrema found near a global maximum/minimum and spaces with discontinuities in the figure of merit and its gradient. The smoothly varying parameter space with a single, global maximum, seen in the calculated Q results of the parameter sweeps in Fig. 2, suggests GO would be a more appropriate choice for optimizing the mixed unit cell PhCs explored here. To verify this hypothesis, we investigated a gradient approach to optimize the bowtie unit cell dimensions with coarse parameter sweep simulation data from Fig. 2(a, c). The design optimization paths for both of the previously simulated PhC nanobeam cavities are shown in Fig. 3. Figure 3(a) shows GO for the air hole-bowtie design starting from an initial choice of bowtie unit cell geometry with the same radius and unit cell width as the central cavity unit cell of the uniform air hole design. It is apparent that this initial guess (circled in red) to maintain radius and unit cell width starts the optimization process at a point in the parameter space located relatively far from the optimal design (circled in blue); however, the GO algorithm was able to arrive at the global maximum in only 5 optimization iterations. Figure 3(b) shows GO for the antislot-bowtie design, starting from an initial guess of the cavity dimensions from the uniform antislot design and resulting in only 2 optimization iterations. We believe that fewer optimization iterations were required for the antislot-bowtie PhC because the mode distribution within the antislot unit cell more closely resembles the mode distribution of the bowtie unit cell than does the circular air hole. Each optimization iteration requires three simulations, one to calculate the Q of the simulation point, and two to compute the derivatives of the Q with respect to the radius and unit cell width. These Q derivatives were approximated by increasing the parameter by a Δ of 5 nm on an interpolated grid of the parameter space and computing ΔQ. This results in a total of 15 simulations needed in Fig. 3(a) and 6 simulations needed in Fig. 3(b), which are both significantly lower than the 121 simulations used to sample the entire parameter space with a 4 nm grid. Hence, for mixed unit cell designs similar to those studied in this work, a gradient-based optimization strategy should enable functional unit cell parameters to be optimized in a computationally efficient manner.

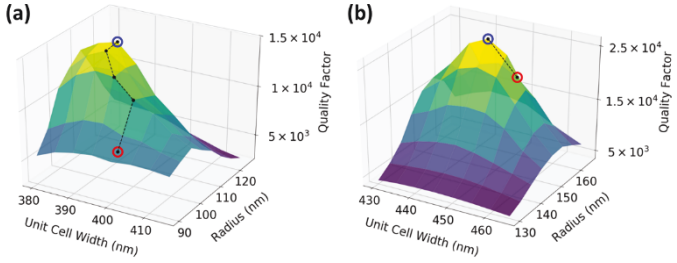

Fig. 3. Gradient optimization illustrated with the parameter spaces simulated in Fig. 2(a, c) starting from bowtie unit cell dimensions of the same radius and unit cell width as the uniform PhC cavity designs. Optimization of calculated Q for (a) the air hole-bowtie PhC nanobeam with initial bowtie radius of 93 nm and unit cell width of 400 nm, requiring 5 iterations, and (b) the antislot-bowtie PhC nanobeam with initial bowtie radius of 160 nm and unit cell width of 450 nm, requiring 2 iterations. The initial point is indicated in red and the converged solution is indicated in blue.

Examining the full parameter space in Fig. 2, it can be seen that the Q can change by nearly one order of magnitude and the resonance wavelength can vary by more than 20 nm when the bowtie unit cell width and radius are tuned over a range of 40 nm each. Interestingly, if having the highest possible Q factor is not necessary for a particular application, the results in Fig. 2 show that a wide range in resonance

wavelengths is achievable for mixed unit cell PhCs by simply tuning the single bowtie unit cell. For the air hole-bowtie design, maximum Q occurs with a bowtie radius of 109 nm and unit cell width of 390 nm. For the antislot-bowtie design, these values are 155 nm and 444 nm, respectively. To properly capture the mode confinement at the ultrasmall "knot" in the center of the bowtie, the Q and V_m values are calculated using FDTD simulations with non-uniform, 3 nm meshing locally in the region surrounding the knot of the bowtie. The air hole-bowtie PhC has $Q = 1.2\times10^4$ and $V_m = 1.6\times10^{-4}\ (\lambda/n_{air})^3$ at a wavelength of 1515 nm, and the antislot-bowtie PhC has $Q = 2.7\times10^4$ and $V_m = 2.2\times10^{-4}\ (\lambda/n_{air})^3$ at a wavelength of 1549 nm. These simulated values, along with those of the comparably simulated (i.e., with similar meshing) uniform designs discussed earlier, are summarized in Table 1. For reference, we also include in Table 1 the simulated Q and V_m values for a uniform all-bowtie PhC nanobeam (Fig. 1(a)) with the same number of unit cells as the antislot PhC and a taper in radius from 150 nm to 170 nm. The fundamental resonance for this all-bowtie PhC is located at 1555 nm. It is clear from these results that while the Q of the mixed unit cell PhCs is mildly impacted by the inclusion of the bowtie unit cell, the reduction in mode volume by two orders of magnitude improves the Q/V_m metric dramatically and demonstrates the utility of the mixed unit cell designs, especially with regards to nonlinear optics, advanced sensing, and enhanced quantum emission [12]. While the V_m is similar in all designs with a bowtie at the center of the cavity because the bowtie shape is critical for enabling ultra-low V_m, it is important to note that the Q for all types of PhC nanobeam cavities depends primarily on the number of unit cells and how they are tapered along the nanobeam. Therefore, Q values higher than what we report here are possible by including longer tapers and more maximum mirror strength unit cells.

Table 1. Simulated Q and V_m for Mixed Unit Cell PhC Designs

Device	Q	$V_m\ (\lambda/n_{air})^3$
Air Hole-Air Hole	7.9×10^4	1.5×10^{-2}
Air Hole-Bowtie	1.2×10^4	1.6×10^{-4}
Antislot-Antislot	9.4×10^4	2.8×10^{-2}
Antislot-Bowtie	2.7×10^4	2.2×10^{-4}
Bowtie-Bowtie	1.6×10^5	1.9×10^{-4}

The two primary loss mechanisms in a mixed unit cell PhC nanobeam are expected to be air band edge frequency mismatch and mode profile (or impedance) mismatch, the former reducing the effectiveness of the mirrors at the resonant frequency and the latter producing scattering losses at the interfaces between unit cells. Regardless of the optimization method being used, the optimized designs should reflect the intuitive theory of mode coupling between adjacent unit cells. Optimization in Q for both air hole-bowtie and antislot-bowtie designs in Fig. 2 and 3 show a decrease in the bowtie unit cell width from the period of their respective PhCs. Intuitively, this trend can be understood by considering that the period (a) is related to the vacuum wavelength and effective index (n_{eff}) by $a = \lambda_0/2n_{eff}$, which implies that n_{eff} is larger for the bowtie than the surrounding unit cells. Hence, at a fixed radius, a decrease in the period at the bowtie unit cell (i.e., bowtie unit cell width) is consistent with the principle that the period must be lowered to account for the increased n_{eff} at the same wavelength, λ_0. However, the situation is more complicated when both the radius and width of the bowtie unit cell are varied because the wavelength of the resonance is related to both of these parameters, scaling according to $\lambda \sim a/r$, which can be observed in Fig. 2(b, d). The radius of the bowtie unit cell in the mixed unit cell designs must be tuned, as there is a particular radius that produces the best matched air band edge wavelength between the default and functional unit cells. Since the unit cell width and radius cannot truly be tuned independently, it is necessary to find a numerical solution that results in the most efficient coupling of the guided mode between the bowtie cavity and the surrounding mirror segments.

3. EXPERIMENTAL RESULTS

To experimentally validate the mix-and-match design approach, mixed unit cell PhCs with antislot mirror segments surrounding a bowtie cavity unit cell were fabricated on a silicon-on-insulator wafer with a 220 nm silicon device layer and 3 μm buried oxide layer using standard electron beam lithography and reactive ion etching protocols. In a second lithography step, SU-8 polymer mode couplers were added to improve end-fire coupling efficiency to the PhC nanobeam from the lensed fiber tip used in experimental measurements. Figure 4(a) shows a scanning electron microscope (SEM) image of a representative fabricated PhC nanobeam with mixed unit cells. Transmission characterization was carried out on a device with 12 tapering unit cells and 3 end mirror segments using TE-polarized light from a fiber-coupled tunable laser source (Santec TSL-510), tapered fibers (OZ Optics), and a fiber-coupled optical power meter (Newport 2936-C). Figure 4(b) shows the measured transmission spectrum with three resonances appearing within the measurement window. The resonance at 1579 nm has a Q of ~4×10^3. The difference in resonance wavelength compared to the simulation is attributed to the dimensions of the fabricated structure differing from those in the simulation and to a different number of tapering unit cells. Fabrication of the bowtie geometry relies on achieving feature sizes as small as 10 – 15 nm at the "knot." We utilized careful multilayer dosing of the bowtie and surrounding features to control the inter-shape proximity effect. While care needs to be taken to fabricate this geometry, the mix-and-match PhC design reduces the number of ultrafine features that get patterned and increases the overall device yield. Moreover, a high-Q resonance can still be achieved even if overexposure of the bowtie knot were to cause an opening in the middle; in fact, an opening at the knot of the bowtie would benefit applications involving, for example, the placement of a quantum dot in the bowtie.

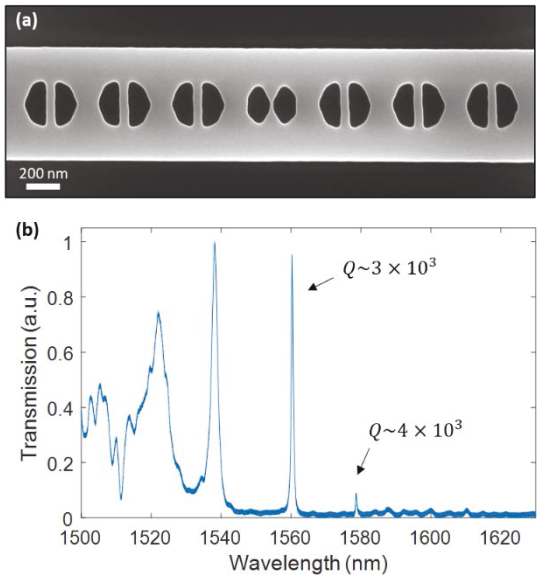

Fig. 4. (a) SEM image of fabricated mix-and-match PhC with a single bowtie unit cell in the center of a 1D PhC composed of antislot unit cells. (b) Transmission measurement of mix-and-match PhC with a loaded Q ~ 4×10^3.

4. CONCLUSION

In conclusion, we have shown, through simulation and experiment, a PhC nanobeam cavity that combines the bowtie unit cell geometry with non-bowtie unit cells for low mode volume resonances, demonstrating a method for designing mixed unit cell PhC nanobeams. The achievement of mixed unit cell PhCs is facilitated by the fact that air-mode resonances in PhC nanobeams allow flexibility in adding subwavelength-sized features within the air hole unit cells. Mixing and matching unit cells in a PhC nanobeam provides the PhC designer with enhanced control in crafting the mode distribution across and within individual unit cells to achieve specialized functionality while balancing other competing interests, such as ease of fabrication and loss-loss operation. Our designed mixed unit cell configuration with antislot unit cells and a bowtie cavity gives high Q/V_m performance ($Q \sim 10^4$, $V_m \sim 10^{-4}\,(\lambda/n_{air})^3$) while reducing fabrication complexity.

Funding Information. National Science Foundation (NSF) (ECCS1407777 and ECCS1809937); BUPT Excellent Ph.D. Students Foundation (CX2016207); National Science Foundation Graduate Research Fellowship (F. O. Afzal).

Acknowledgment. Fabrication was conducted at the Center for Nanophase Materials Sciences, a DOE Office of Science User Facility. The authors thank D. P. Briggs, K. C. Lester, and S. T. Retterer for assistance with sample fabrication. SEM imaging and technical support at the Vanderbilt Institute for Nanoscale Science and Engineering is also acknowledged.

Disclosures. The authors declare no conflicts of interest.

References

1. M. Soljačić, S. G. Johnson, S. Fan, M. Ibanescu, E. Ippen, and J. D. Joannopoulos, "Photonic-crystal slow-light enhancement of nonlinear phase sensitivity," J. Opt. Soc. Am. B **19**, 2052 (2002).
2. K. Nozaki, T. Tanabe, A. Shinya, S. Matsuo, T. Sato, H. Taniyama, and M. Notomi, "Sub-femtojoule all-optical switching using a photonic-crystal nanocavity," Nat. Photonics **4**, 477–483 (2010).
3. B. Ellis, M. A. Mayer, G. Shambat, T. Sarmiento, J. Harris, E. E. Haller, and J. Vučković, "Ultralow-threshold electrically pumped quantum-dot photonic-crystal nanocavity laser," Nat. Photonics **5**, 297–300 (2011).
4. K.-Y. Jeong, Y.-S. No, Y. Hwang, K. S. Kim, M.-K. Seo, H.-G. Park, and Y.-H. Lee, "Electrically driven nanobeam laser," Nat. Commun. **4**, 2822 (2013).
5. M. R. Lee and P. M. Fauchet, "Two-dimensional silicon photonic crystal based biosensing platform for protein detection," Opt. Express **15**, 4530 (2007).
6. W.-C. Lai, S. Chakravarty, Y. Zou, Y. Guo, and R. T. Chen, "Slow light enhanced sensitivity of resonance modes in photonic crystal biosensors," Appl. Phys. Lett. **102**, 041111 (2013).
7. S. Hu and S. M. Weiss, "Design of Photonic Crystal Cavities for Extreme Light Concentration," ACS Photonics **3**, 1647–1653 (2016).
8. H. Choi, M. Heuck, and D. Englund, "Self-Similar Nanocavity Design with Ultrasmall Mode Volume for Single-Photon Nonlinearities," Phys. Rev. Lett. **118**, 223605 (2017).
9. S. Hu, M. Khater, R. Salas-Montiel, E. Kratschmer, S. Engelmann, W. M. J. Green, and S. M. Weiss, "Experimental realization of deep-subwavelength confinement in dielectric optical resonators," Sci. Adv. **4**, eaat2355 (2018).
10. P. Seidler, K. Lister, U. Drechsler, J. Hofrichter, and T. Stöferle, "Slotted photonic crystal nanobeam cavity with an ultrahigh quality factor-to-mode volume ratio," Opt. Express **21**, 32468 (2013).
11. S. I. Halimi, Z. Fu, F. O. Afzal, J. A. Allen, S. Hu, and S. M. Weiss, "Photonic Crystal Design with Mix and Match Unit Cells for Mode Manipulation," in *Conference on Lasers and Electro-Optics* (OSA, May 6th, 2019), p. SM2J.4.
12. H. Choi, D. Zhu, Y. Yoon, and D. Englund, "Cascaded Cavities Boost the Indistinguishability of Imperfect Quantum Emitters," Phys. Rev. Lett. **122**, 183602 (2019).
13. Q. Quan, P. B. Deotare, and M. Loncar, "Photonic crystal nanobeam cavity strongly coupled to the feeding waveguide," Appl. Phys. Lett. **96**, 203102 (2010).
14. Q. Quan and M. Loncar, "Deterministic design of wavelength scale, ultra-high Q photonic crystal nanobeam cavities," Opt. Express **19**, 18529 (2011).
15. P. Lalanne and J. P. Hugonin, "Bloch-wave engineering for high-Q, small-V microcavities," IEEE J. Quantum Electron. **39**, 1430–1438 (2003).
16. C. Sauvan, G. Lecamp, P. Lalanne, and J. P. Hugonin, "Modal-reflectivity enhancement by geometry tuning in Photonic Crystal microcavities," Opt. Express **13**, 245–255 (2005).
17. J. D. Joannopoulos, S. G. Johnson, J. N. Winn, and R. D. Meade, *Photonic Crystals: Molding the Flow of Light*, 2nd ed. (Princeton University Press, 2008).
18. V. R. Almeida, Q. Xu, C. A. Barrios, and M. Lipson, "Guiding and confining light in void nanostructure," Opt. Lett. **29**, 1209 (2004).
19. S. I. Halimi, S. Hu, F. O. Afzal, and S. M. Weiss, "Realizing high transmission intensity in photonic crystal nanobeams using a side-coupling waveguide," Opt. Lett. **43**, 4260 (2018).
20. Y. Zhang, S. Yang, A. E.-J. Lim, G.-Q. Lo, C. Galland, T. Baehr-Jones, and M. Hochberg, "A compact and low loss Y-junction for submicron silicon waveguide," Opt. Express **21**, 1310 (2013).
21. M. Minkov, V. Savona, and D. Gerace, "Photonic crystal slab cavity simultaneously optimized for ultra-high Q / V and vertical radiation coupling," Appl. Phys. Lett. **111**, 131104 (2017).
22. J. S. Jensen and O. Sigmund, "Topology optimization for nano-photonics," Laser Photon. Rev. **5**, 308–321 (2011).
23. C. M. Lalau-Keraly, S. Bhargava, O. D. Miller, and E. Yablonovitch, "Adjoint shape optimization applied to electromagnetic design," Opt. Express **21**, 21693 (2013).
24. A. Y. Piggott, J. Lu, K. G. Lagoudakis, J. Petykiewicz, T. M. Babinec, and J. Vucković, "Inverse design and demonstration of a compact and broadband on-chip wavelength demultiplexer," Nat. Photonics **9**, 374–377 (2015).